Chalcogenide Letters Vol. 20, No. 7, July 2023, p. 515 - 533

Impact of TeO_2-B_2O_3 manipulation on optical and radiation shielding properties of mixed glass former borotellurite glass

D. Said[a], N. M. Samsudin[a], M. M. Naaim[a], M. I. Sayyed[b], M. H. M. Zaid[c], M. N. Azlan[d], S. M. Iskandar[e], N. N. Yusof[e], E. S. Sazali[f], R. Hisam[a,*]
[a]*Faculty of Applied Sciences, Universiti Teknologi MARA, 40450 Shah Alam, Selangor, Malaysia*
[b]*Department of Physics, Faculty of Science, Isra University, Amman – Jordan*
[c]*Department of Physics, Faculty of Science, Universiti Putra Malaysia, 43400 Serdang, Selangor, Malaysia*
[d]*Physics Department, Faculty of Science and Mathematics, Universiti Pendidikan Sultan Idris, 35900 Tanjong Malim, Perak, Malaysia*
[e]*School of Physics, Universiti Sains Malaysia, 11800 USM, Penang, Malaysia*
[f]*Advanced Optical Materials Research Group, Department of Physics, Faculty of Science, Universiti Teknologi Malaysia, Skudai, Johor 81310, Malaysia*

(80-x)B_2O_3-$x$$TeO_2-10Li_2O$-$Al_2O_3$ (x=10-60 mol%) mixed glass former (MGF) glasses were prepared by using melt-quenching method to investigate the effect of mixed glass former between B_2O_3 and TeO_2 on the optical properties and to evaluate the radiation shielding ability of the glass. Extremes observed at x=40 mol% for all optical properties' parameters were suggested due to large number of non-bridging oxygen. The radiation shielding properties of the glass samples were determined for 0.284 MeV–1.333 MeV energy range by using Phy-X/PSD software. The studied radiation parameters have shown enhancement due to high density and high atomic number, Z of Te over B.

(Received May 8, 2023; Accepted July 24, 2023)

Keywords: Borotellurite, Optical properties, Radiation shielding, Mixed glass former

1. Introduction

Oxide glasses have been substantially explored because of their excellent advantages such as easy-production and glorious physical as well as chemical properties of glasses which have intrigued the mind of researchers and industrial players toward the amorphous solids over crystalline materials [1-3]. Besides that, multiple unique traits of glasses also have made glasses such a good potential for noble optical devices [4-6]. Oxide glasses can be categorized into three groups namely former, intermediate and modifier based on their single bond strength value [7]. Recently, composing a glass with two glass former has been a special focus among the research community as the approach is believes to improve the properties of the glass. Interestingly, this approach of mixing two glass formers whilst other constituent be at constant molar amount has create an anomalous behavior which later addressed as the mixed glass former effect or MGFE [8]. Particularly, borotellurite MGF glass which from borate and tellurite are expected to be significantly important in the fast-pace technological and industrial demands especially in laser and solid electrolytes applications [9].

On one hand, borate (B_2O_3) is known to be the best glass former due to its wide array of advantages such as low melting point, high toughness, low viscosity and reliable chemical-withstand [6, 10, 11]. It comprises of two functional groups of trigonal-BO_3 and four-fold-BO_4 in boroxol ring with various superstructural units such as tri-, penta-, tetra-, di-, pyro- and ortho-borate [7]. Additionally, the introduction of glass modifier such as alkali or alkaline group will modify the structure through the evolution of those two functional groups [12, 13]. On the other hand, tellurite (TeO_2) is a conditional glass former which need assist from the modifier to make up

* Corresponding author: rosdiyana@uitm.edu.my
https://doi.org/10.15251/CL.2023.207.515

the glass structure through enhancing glass forming ability. TeO_2 has numerous remarkable advantages such as high refractive index, non-hygroscopic, high thermal stability and good mechanical strength [14-16]. TeO_2 consist of trigonal bypyramid-TeO_4 and trigonal pyramid-TeO_3 unit structure with a lone pair at the equatorial position [17]. Combining these two glass formers at a proper ratio will potentially maximize the inner potential and efficiency whilst reduce the flaw. Presence of these two glass formers will interestingly influence the glass network conductivity which consequently affecting the structural and optical properties of the glass systems.

Previous optical studies on MGF glass systems have produced different kinds of results. An optical study conducted on $20Li_2O$-$(80-x)Bi_2O_3$-$xSiO_2$ MGF glass system has unexpectedly resulted in a monotonous pattern where the optical band gap, E_{opt} were increased whilst optical basicity, Λ and electronic polarizability, $\alpha_{O^{2-}}$ were decreased with increasing SiO_2 [18]. This was suggested to due to the plunge in BiO_6 octahedral units which is a non-bridging oxygen (NBO) unit. However, an opposite monotonous behavior was observed in $10ZnO$-xBi_2O_3-$(90-x)B_2O_3$ MGF glass system where increasing Bi_2O_3 content has exhibited a decrease in E_{opt} as well as an increase in the Λ and $\alpha_{O^{2-}}$ in which these occurrences were attributed to the increase in the formation of NBO [19]. In the meantime, a non-linear behavior of optical properties was also observed in certain MGF glass system. For example, the $30Li_2O$-$20ZnO$-xBi_2O_3-$(50-x)B_2O_3$ MGF glass system has depicted a decrease with an anomalous at 40 mol% [12]. It was suspected to be due to the role-changing behavior of Bi_2O_3 from a modifier to a former which produces lesser number of NBO as Bi_2O_3 increases. This situation was also reflected and coincided with other parameter such as the Urbach Energy (E_u), Λ and $\alpha_{O^{2-}}$; hence, it was suggested to be related to the MGFE influence. Overall, the contradictory, multi-kind obtained results have emphasized that the issue of MGF glass system is still scarce and not well-elucidated; thus, further investigation is much needed for better enlightenment.

Prolonged overexposure to radiation or nuclear accident might lead to severe consequences as well as casualties. Current lead-based material is highly toxic whereas various kind of concrete are prone to crack, heavy, immobile and non-transparent [22-24]. Recently, oxide glasses have attracted attentions as alternatives in radiation shielding that edges other materials with their magnificent qualities such as affordability, high transparency and portability. Specifically, research on MGF glass as radiation shielding material has gained popularity as study was conducted on B_2O_3-Li_2O-P_2O_5-PbO[3] and Bi_2O_3-Li_2O-B_2O_3 [24] MGF glass system with outstanding outcomes. Therefore, addition of TeO_2 into this MGF glass was expected to improve overall shielding power due its high density and high atomic number whilst the presence of Al_2O_3 can upgrade the mechanical strength of the glass. To the date, manipulating borotellurite content with constant amount of modifier is yet to be reported, hence, it is worth to study the potential of borotellurite MGF glass system on the radiation shielding matter.

Nevertheless, this paper attempted to explore the effect of $(80-x)B_2O_3$-$xTeO_2$-$10Li_2O$-Al_2O_3 (x=10-60 mol%) mixed glass former on optical and radiation shielding properties. These properties were investigated by using optical absorption spectroscopy and radiation simulation software. The radiation simulation software was used to determine the crucial radiation shielding parameters such as mass attenuation coefficient (MAC), half-value layer (HVL) and etc.

2. Experimental methods

2.1. Sample preparations

$(80-x)B_2O_3$-$xTeO_2$-$10Li_2O$-Al_2O_3 (x=10-60 mol%) quaternary mixed glass former (MGF) glass system has been prepared by using the conventional melt-quenching technique. An appropriate amount of high purity (>99%) analytical grade commercial chemical powders of Tellurium (IV) Oxide (TeO_2), Boron Oxide (B_2O_3), Lithium Carbonate (Li_2CO_3) and Aluminium Oxide (Al_2O_3) were weighed accordingly with pre-calculated mass and hence, ground by using agate pestle and mortar for approximately 1 hour to achieve fine and homogenous mixture. The fine mixture powder was then transferred into alumina crucible to undergone melting process at 1000C for 3 hours. After that, the molten glass powder was quenched into pre-heated stainless

steel mold and hence, annealed at 350C for 2.5h to reduce any internal mechanical stress of the quenched sample. The sample was eventually cooled to the room temperature. The bulk samples were then crushed into powder form for further sample characterization.

2.2. Sample characterization

2.2.1. Optical absorption spectroscopy

The optical absorption spectroscopy of (80-x)B_2O_3-$x$$TeO_2-10Li_2O$-$Al_2O_3$ (x=10–60 mol%) glass samples was recorded at room temperature in the wavelength range of 200–1100 nm using Double Beam Shimadzu UV-Vis-NIR spectrophotometer.

2.2.2. Radiation shielding

Meanwhile, the radiation shielding parameters of (80-x)B_2O_3-$x$$TeO_2-10Li_2O$-$Al_2O_3$ (x=10–60 mol%) were determined using Phy-X/PSD software for energy range 0.284 MeV–1.333 MeV. Crucial and important parameters were evaluated such as linear attenuation coefficient (LAC), mean free path (MFP), half-value layer (HVL) and many more. The interaction between photon and glasses' atom via attenuation and absorption were discussed.

3. Results and discussions

3.1. Optical absorption spectroscopy

Optical study is very useful to elucidate the optically-induced electronic transitions and provide information on energy gap and band structure of material which is closely related to glass network modification. Fundamental absorption edge corresponds to the electronic transition from valence to conduction band which require minimum energy for the excitation [20]. The absence of sharp absorption edge along the optical absorption spectra as a function of the wavelength of (80-x)B_2O_3-$x$$TeO_2-10Li_2O-10Al_2O_3$ (x =10−60 mol%) glass samples (Figure 1) further confirms the amorphous nature of the samples.

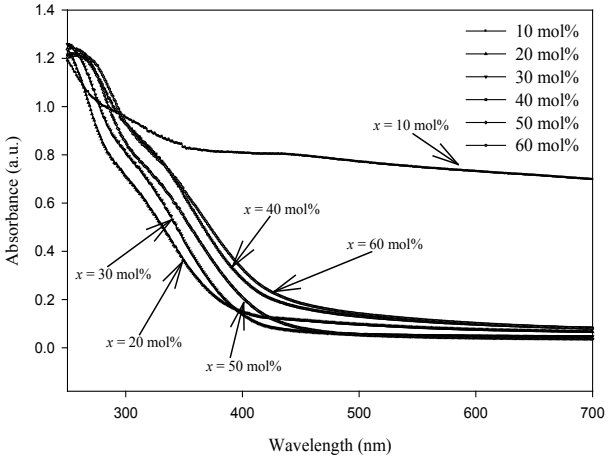

Fig. 1. Plot of UV-Vis-NIR absorption spectra of (80-x)B_2O_3-xTeO_2-10Li_2O-10Al_2O_3 (x=10−60 mol%) glass samples.

Optical band gap, E_{opt} is the forbidden region between valence band and conduction band. When electromagnetic waves in the UV-Vis-IR region are absorbed by the electrons in the valence band maximum, they will jump to minimum conduction band if the energy absorbed is enough. The values of E_{opt} between valence and conduction bands are discrete for each material which can be explained by the behavior of optical absorption edge of the optically induced transition type. Optical transitions and electronic band structures in amorphous and crystalline materials can be investigated using UV-Vis-NIR absorption spectroscopy method [21, 22]. For oxide glasses, direct

and indirect optical transition can occur at the fundamental absorption edge, which obeys selection rules. Direct transitions are the electronic transition from the maximum valence band to minimum conduction band located at the same K value, while indirect transitions show the maximum valence and minimum conduction band occurred at different K values [22, 23]. The changes in direct and indirect E_{opt} can be understood by the changes in NBOs number, structural changes, and chemical bonding with addition of TeO_2 [24, 25].

E_{opt} of the glass can be determined by using Davis and Mott relation [26]:

$$\alpha(v) = B\left(\frac{(\square v - E_{opt})^n}{\square v}\right) \quad (1)$$

where α is the absorption coefficient, *B* is a constant, *hv* is the incident photon energy, and E_{opt} is the optical energy band gap. The E_{opt} of the samples were obtained from the zero intercept whereby the linear regression on the slope of the linear region of the plot of $(\alpha hv)^{1/n}$ on the y-axis versus photon energy *(hv)* in eV on the x-axis meets the zero $(\alpha hv)^{1/n}$. However, this study has employed Kubelka-Munk (K-M) method that offers a great advantage to a highly light scattering materials and absorbing particles in a matrix that is where *F(R)* is corresponds to absorption coefficient (α):

$$F(R) = \frac{(1-R)^2}{2R} \quad (2)$$

where R is the reflectance value obtained from UV-Vis-NIR data and hence, the equation (1) has been modified to become:

$$(F(R)hv) = B\left(hv - E_{opt}\right)^n \quad (3)$$

The modified K-M plots were plotted for various values of n, that is, 1/2, 2, 1/3, and 3 corresponding to direct allowed, indirect allowed, direct forbidden, and indirect forbidden transitions, respectively. For amorphous materials, the indirect (plotted as $(F(R)hv)^{1/2}$ versus *hv*) and direct (plotted as $(F(R)hv)^2$ versus *hv*) allowed transition corresponding to n=2 and n=1/2 [7, 27].

The variations of E_{opt} with TeO_2 addition are shown in Figure 2 and 3, while the values are listed in Table 1. Values of the E_{opt} lies in the range of 3.23−3.84 eV for direct allowed transition and 4.15−4.54 eV for indirect allowed transition, respectively (Table 1) which is quite close to that found in boro-tellurite glasses, such as $(60\text{-}x)B_2O_3$-$(10+x)TeO_2$-10ZnO-$10Al_2O_3$-$5Li_2O$-5MgO [25] and $\{((TeO_2)_{0.70}(B_2O_3)_{0.30})_{1-x}(ZnO)x\}_{1-y}(Er_3O_2)_y$ [24]. Non-linear increase in E'_{opt} is seen for direct allowed optical band gap. E'_{opt} initially increased at high rate from 3.28 eV (*x*=10 mol%) to 3.84 eV (*x*=20 mol%) but begin to drastically decrease to 3.64 eV (*x*=30 mol%) and reach minimum at *x*=40 mol% TeO_2 at 3.23 eV (Figure 4). However, for *x*>40 mol% TeO_2, E'_{opt} started to increase to 3.58 eV (*x*=50 mol%) before decreased to 3.36 eV (*x*=60 mol%). Meanwhile, it is seen that for indirect allowed transition, E''_{opt} exhibits almost similar trend with direct transition at *x*>40 mol%. E''_{opt} initially decreased from 4.54 eV (*x*=10 mol%) to 4.18 eV at *x*=40 mol% TeO_2. For *x*>40 mol% TeO_2, E''_{opt} shows similar trend with direct transition, whereby it started to increase to 4.25 eV (*x*=50 mol%) before decreased to 4.15 eV (*x*=60 mol%).

The initial increase in E'_{opt} for $x \leq 20$ mol% is suggested to be due to the increase in BO formation via TeO_4 and AlO_4. Meanwhile, the decrease of E'_{opt} and E''_{opt} to a minimum at *x*=40 mol% (Figure 4) was strongly influenced by a large number of NBOs formation via TeO_3 and BO_3 units resulting from strong competition between both B_2O_3 and TeO_2 glass formers which is destructive to the glass network [23, 28, 29]. Previous study reported that NBO has higher polarizability than BO, thus NBO binds excited electrons less tightly than BO. Hence, NBO's electrons require less energy to induce electron excitation than BO's electrons leading to the decrease in E'_{opt} and E''_{opt} with an increase in NBO [28, 30, 31]. Moreover, a large NBO ion indicates in shifting of valence band maximum to higher energies, which result to a smaller optical energy gap [12, 29, 32]. On the other hand, the increase in E'_{opt} and E''_{opt} for *x*>40 mol% is attributed to the increase in formation of BO via BO_4 units. The minimum in E'_{opt} and E''_{opt} at *x*=40 mol% indicate that this quantity was also affected by the MGFE.

Table 1. Values of direct, E'_{opt} and indirect, E''_{opt} allowed optical band gap, direct, n' and indirect, n'' allowed E_{opt} based-refractive index and Urbach energy (E_u) for (80-x)B_2O_3-xTeO_2-10Li_2O-10Al_2O_3 (x = 10−60mol%) glass samples.

x (mol %)	Direct allowed transition n = ½, $\boldsymbol{E'_{opt}}$ (eV)	*n'* (direct)	Indirect allowed transition n = 2, $\boldsymbol{E''_{opt}}$ (eV)	*n''* (indirect)	E_u (eV)
10	3.28	2.325	4.54	2.072	0.95
20	3.84	2.201	4.53	2.075	0.43
30	3.64	2.244	4.38	2.099	0.48
40	3.23	2.338	4.18	2.136	0.66
50	3.58	2.257	4.25	2.124	0.46
60	3.36	2.306	4.15	2.142	0.53

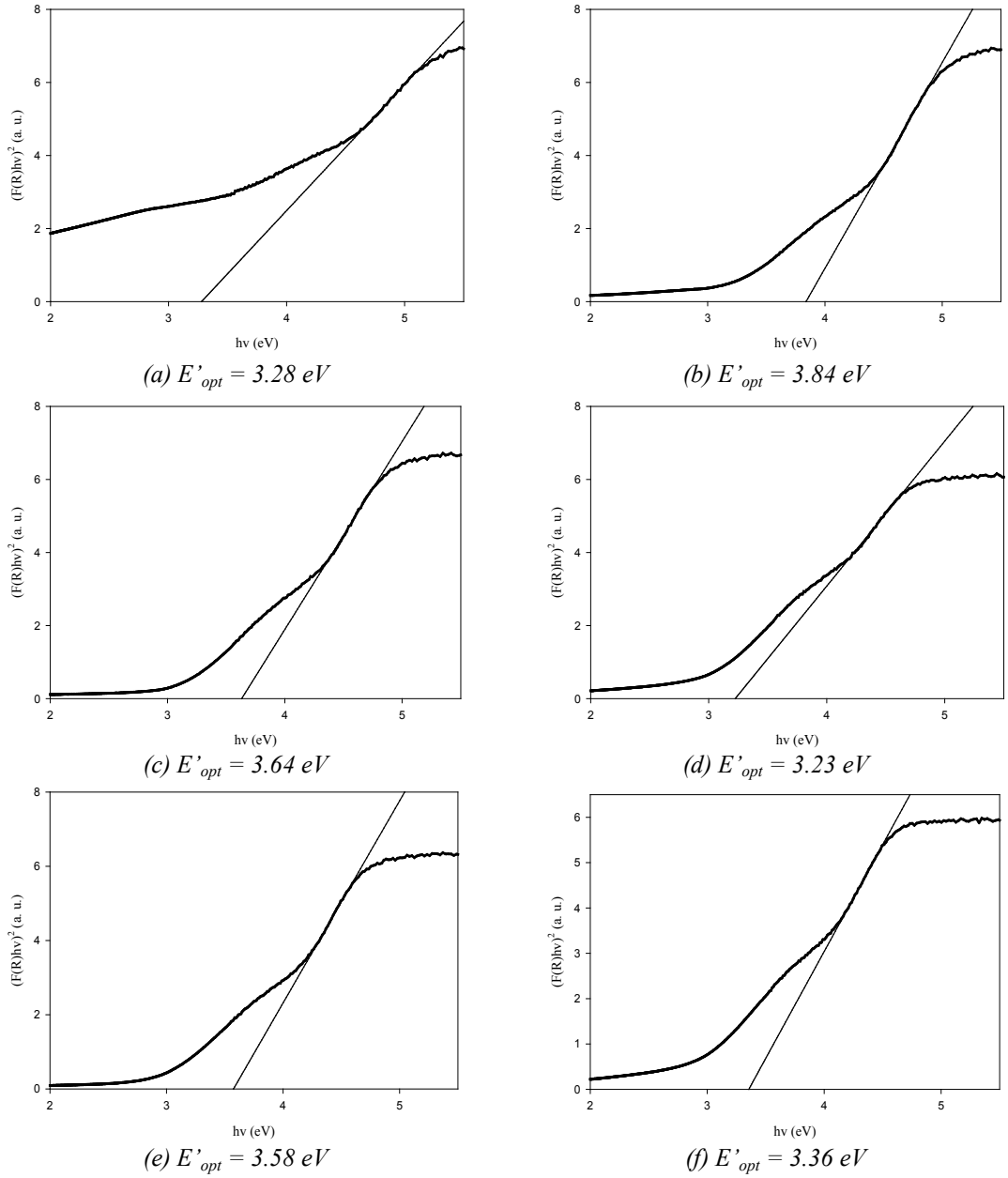

(a) E'$_{opt}$ = 3.28 eV *(b) E'$_{opt}$ = 3.84 eV*

(c) E'$_{opt}$ = 3.64 eV *(d) E'$_{opt}$ = 3.23 eV*

(e) E'$_{opt}$ = 3.58 eV *(f) E'$_{opt}$ = 3.36 eV*

Fig. 2. Plots of $(\alpha hv)^2$ against (hv) of (80-x)B_2O_3-xTeO_2-10Li_2O-10Al_2O_3 (x=10−60 mol% for (a) to (f), respectively) glass samples.

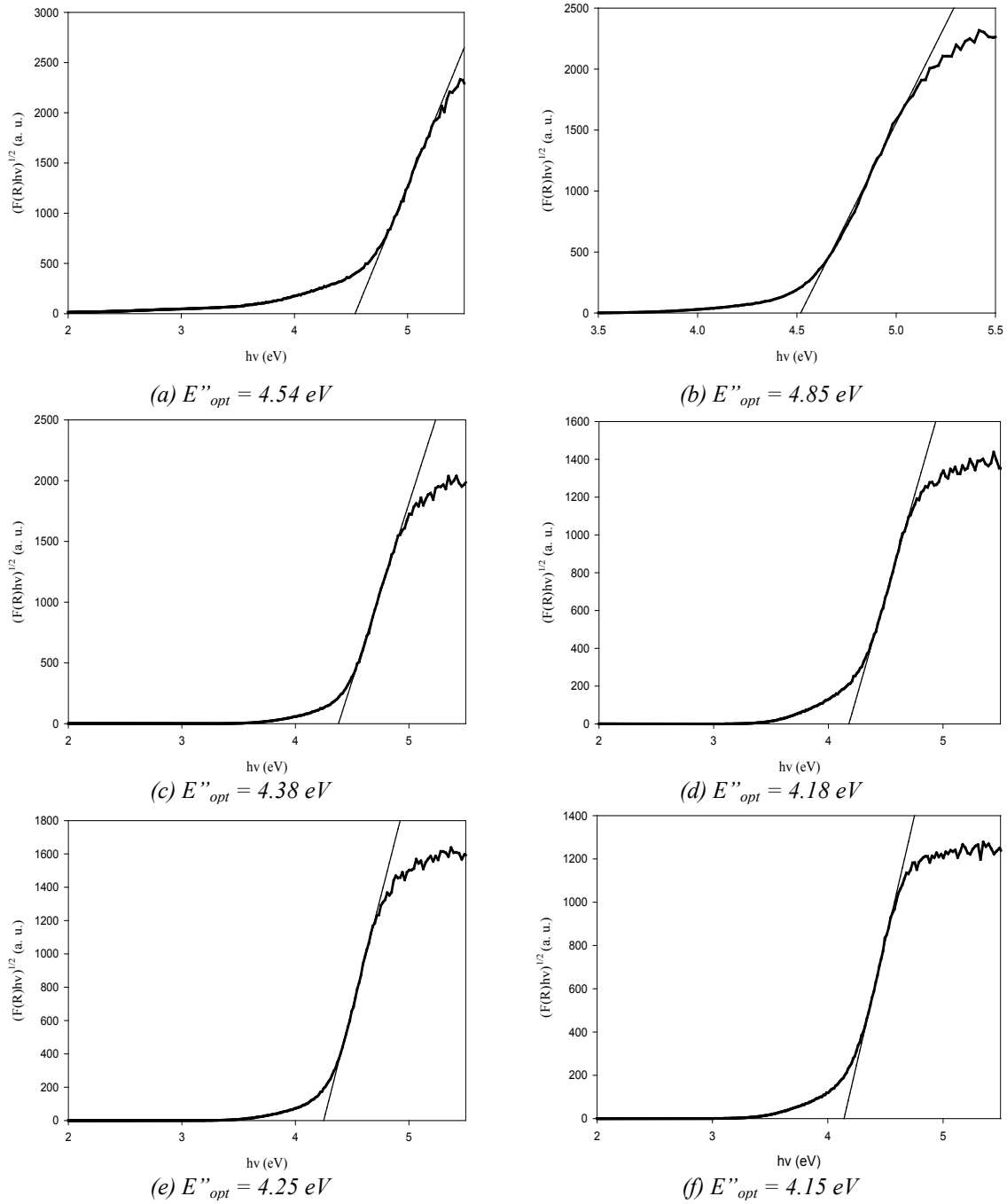

(a) E"$_{opt}$ = 4.54 eV

(b) E"$_{opt}$ = 4.85 eV

(c) E"$_{opt}$ = 4.38 eV

(d) E"$_{opt}$ = 4.18 eV

(e) E"$_{opt}$ = 4.25 eV

(f) E"$_{opt}$ = 4.15 eV

Fig. 3. Plots of $(\alpha hv)^{1/2}$ against (hv) of $(80\text{-}x)B_2O_3\text{-}xTeO_2\text{-}10Li_2O\text{-}10Al_2O_3$ (x=10−60 mol% for (a) to (f), respectively) glass samples.

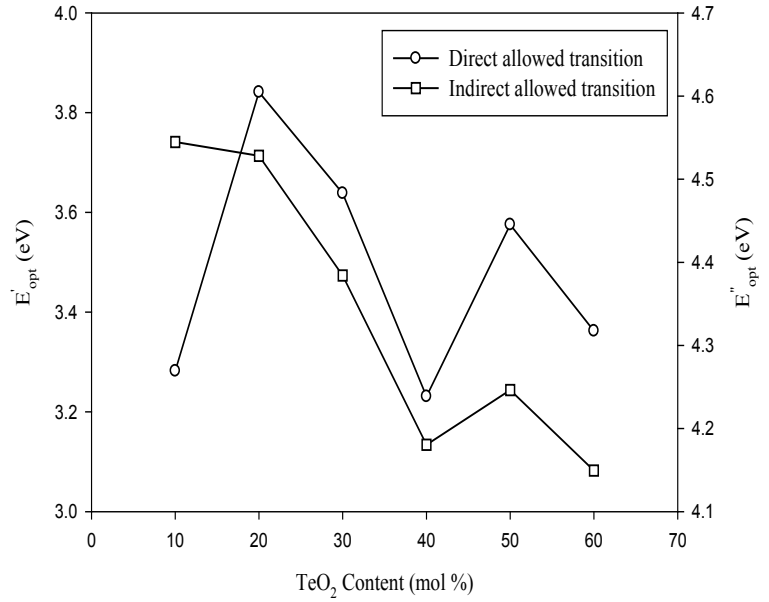

Fig. 4. Plots of Direct, E'opt and Indirect, E"opt with TeO_2 Content for (80-x)B_2O_3-xTeO2-10Li_2O-10Al_2O_3 (x = 10−60 mol%) glass samples.

Refractive index, *n* of a glass corresponds to the interaction between electromagnetic rays with NBOs' electrons of the glass [24, 32]. It was suggested that *n* of glass can also be affected by electronic polarizability of oxide ion at optical frequencies and optical basicity Direct and indirect allowed E_{opt} based-*n* were calculated using the following equation [33, 34]:

$$\frac{n^2-1}{n^2+2} = 1 - \sqrt{\frac{E_{opt}}{20}} \tag{4}$$

Compared to direct allowed E_{opt}, *n* shows an opposite trend (Figure 5) where *n* initially decreased from 2.32 (*x*=10 mol%) to 2.20 (*x*=20 mol%) before starting to increase to a maximum of 2.34 at *x*=0.4 mol%. However, for *x*>40 mol%, the *n* values dropped drastically to 2.26 (*x*=50 mol%) before rapidly increased to 2.31 (*x*=60 mol%). On the other hand, for indirect allowed E_{opt} based-refractive index, the values show linear increase with the addition of TeO_2 (*x*=10-40 mol%) from 2.072 to 2.136, respectively. For *x*>40 mol%, the values follow similar trend with direct *n* which rapidly decreased to 2.124 (*x*=50 mol%) before a large increased to 2.142 (*x*=60 mol%).

The initial decrease in *n* (*x*≤20 mol%) for direct transitions was suggested to be due to the presence of high BO via TeO_4 units. The massive increase in *n* especially in the MGFE region (*x*≤40 mol%) where a maximum was seen at *x*=40 mol% for both transitions (Figure 5) was suggested to be due to the increase in NBO formation via TeO_3 and BO_3 units, which possessed higher polarizability than BO [17, 35]. Meanwhile, for *x*≥50 mol%, *n* was observed to increase with decrease in NBO formation. This can be suggested by the high concentration of TeO^{4+} ions which possessed higher cation polarizability (0.242 $Å^3$) than B^{3+} ions (0.002 $Å^3$) that increases the polarizability of the glass thus supporting the increase in *n* [35, 36].

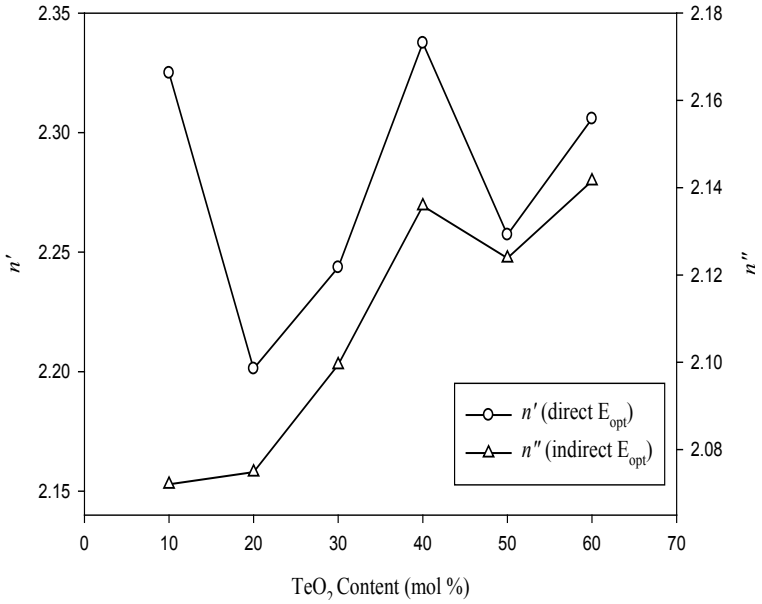

Fig. 5. Plots of direct, n' and indirect, n'' allowed E_{opt} based-n with TeO_2 content for (80-x)B_2O_3-xTeO_2-10Li_2O-10Al_2O_3 (x = 10−60 mol%) glass samples.

In non-crystalline materials, different type of optical absorption edge can be observed where absorption still occurred even when the photon energy is less than energy gap. This type of optical absorption edge that involves electrons in the localized state within the energy gap is known as Urbach tail. The Urbach tails are characterized by the band tail parameter of Urbach energy, E_u which exhibits the degree of defects in the glass network [30, 37]. These defects can either be caused by oxygen vacancies due to volatilization loss of oxygen during glass melting or formation of NBO [38, 39]. E_u is calculated based on the following equation [39]:

$$\alpha(hv) = Ce^{\left(\frac{hv}{E_u}\right)} \tag{5}$$

where E_u is the Urbach energy in eV and C is a constant. Then, the values of E_u were obtained from reciprocals of the slope of the linear part of the curve of the plot of ln (α) versus *hv*.

Dielectric constant, ε can be calculated based on the following equation [40, 41]:

$$\varepsilon = n^2 \tag{6}$$

The variations of E_u with TeO_2 content for all glass samples were listed in Table 1. The values of E_u exhibit similar trend with direct allowed E_{opt} based-*n* in which a large decrease is seen from 0.95 eV (*x*=10 mol%) to 0.43 eV (*x*=20 mol%), initially upon TeO_2 addition before it begin to increase rapidly until *x* = 40 mol% (0.66 eV) where anomalous peak is visible. However, for *x*>40 mol%, E_u decreased to 0.46 eV (*x*=50 mol%) before increased to 0.53eV (*x*=60 mol%). The variation of ε was illustrated in Figure 6. The values of ε shows similar trend with E_u in which a large decrease is seen from 4.41 (*x*=10 mol%) to 3.85 (*x*=20 mol%) initially before increasing rapidly to a maximum of 4.46 (*x*=40 mol%). For *x*≥50 mol%, ε decreased to 4.10 before increasing back to 4.32 (*x*=60 mol%).

Urbach energy, E_u corresponds to the width of the localized states (band tail) within the optical band gap which originating from the formation of defects. These defects may come from the presence of NBO or oxygen vacancies as a result of volatilization loss of oxygen during glass melting [4, 28, 30]. A large value of E_u indicates large concentration of defects. The peak of E_u observed at *x*=40 mol% (Figure 6) suggests high defect concentration contributed by large NBO concentration via TeO_3 and BO_3 units. This finding is consistent with our FTIR results [42].

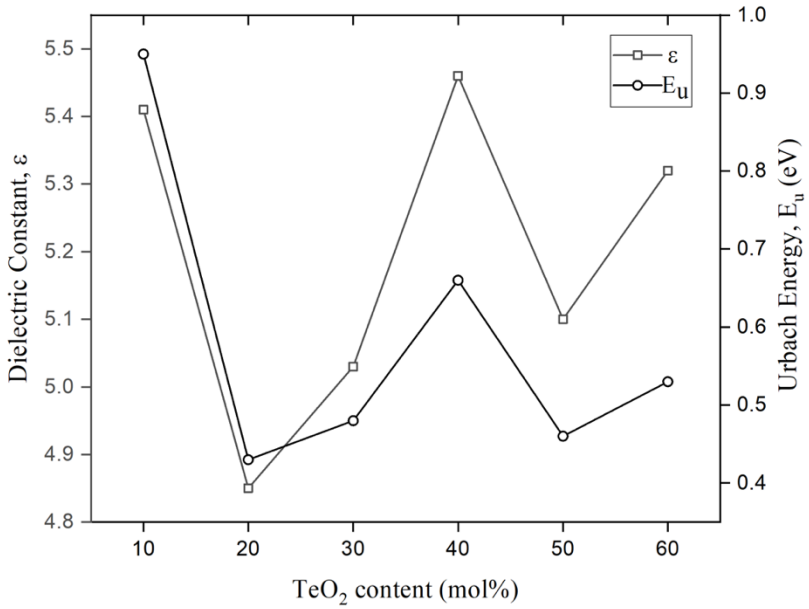

Fig. 6. Plot of ε and E_u with TeO_2 content of (80-x)B_2O_3-xTeO_2-10Li_2O-10Al_2O_3 (x=10−60 mol%) glass samples.

Optical basicity, Λ is the measure of acid-base properties of oxide glasses. In other word, it determines the average electron donating power of oxygen of the oxide species in the glass system. The Λ is a parameter related to the electron donor power of the oxygen in glasses which can be used to estimate the character of bonds present in the glass network. High and low values of Λ corresponds to ionic and covalent characters, respectively [32]. Increase in oxide ion polarizability is related to the increase of electron donor power. Therefore, Λ has close connection with oxide ion polarizability [24].

Meanwhile, the oxide ion electronic polarizability, $\alpha_{O^{2-}}$is directly associated with the deformability of ion's electronic clouds upon applied electromagnetic field [36, 43]. High value of $\alpha_{O^{2-}}$ indicates stronger ability of electron donor of oxide ion. According to Fajan's rule, the polarizability of anion should be decreased in the coulomb field of cation [36]. This is due to the increase in electrostatic potential which came from the increase in positive charge around the anion. Thus, the electron donor power of oxygen atom decreases which in turn increase its covalency. Hence, an increase in NBO formation should decrease anion covalency and increase its polarizability together with optical basicity.

Average $\alpha_{O^{2-}}$can be estimated based on E_{opt} or n for any polycomponent oxide glasses. For quaternary oxide glasses with a general formula of $X_1A_pO_q$-$X_2B_rO_s$-$X_3C_nO_m$-$X_4D_tO_u$ where X_n denotes the molar fraction for each oxide, p, r, n, and t represents the proportion of respective cation atoms and q, s, m and u represents the proportion of oxygen atoms in A_pO_q, B_rO_s C_nO_m and D_tO_u compounds, respectively [7], the E_{opt}-based $\alpha_{O^{2-}}$for each glass is calculated using the following equation [33, 34]:

$$a_{O^{-2}}(E_{opt}) = \left[\frac{V_m}{2.52}\left(1-\sqrt{\frac{E_{opt}}{20}}\right)-\sum a_{cat}\right](N_{O^{-2}})^{-1} \quad (7)$$

where V_a is the molar volume, α_{cat} is the cation polarizability given by $X_1p\alpha_A$-$X_2r\alpha_B$-$X_3n\alpha_C$-$X_4t\alpha_D$ (where molar cation polarizability (α) values of Te^{4+}, B^{3+}, Li^{+} and Al^{3+} ions are $\alpha_{Te} = 1.595$ Å^3, $\alpha_B = 0.002$ Å^3, $\alpha_{Li} = 0.024$ Å^3 and $\alpha_{Al} = 0.054$ Å^3, respectively [33, 36] and $N_{O^{2-}}$ is the number of oxide ions in the chemical formula given by X_1q+X_2s+X_3m+X_4u [36, 44].

Meanwhile, the increase in $\alpha_{O^{2-}}$ is related to the increase of electron donor power; therefore, Λ has close connection with $\alpha_{O^{2-}}$. This relationship can be understood by the equation given as follows [45, 46]:

$$\Lambda\left(E_{opt}\right) = 1.67\left[1 - \left(\frac{1}{\alpha_{O^{2-}(E_{opt})}}\right)\right] \quad (8)$$

The variation of $\alpha_{O^{2-}}$ and Λ were depicted in Figure 7 and Table 2. The $\alpha_{O^{2-}}$ displayed almost linear increasing trend throughout the doping range except at x=20 mol% and x=40 mol% where the trend is interrupted by a drop and slight slope change, respectively. Meanwhile, the trend of Λ is seen to exhibit $\alpha_{O^{2-}}$ where Λ increase almost linearly throughout the doping range except at x=20 mol% and x=40 mol% where the trend is interrupted by a drop and slight slope change, respectively.

Although a large number of NBO via BO_3 units were formed at x=20 mol%, a minimum was observed for both $\alpha_{O^{2-}}$ and Λ. This is suggested to be due to large presence of TeO_4 units that indicates high BO concentration and compactness of the glass network which results in formation of larger cation Coulomb field around anion and reduces polarizability, as compared by FTIR results [42]. Hence, the electron donor power of oxygen was reduced and increase in anion covalency. $\alpha_{O^{2-}}$ and Λ showed almost linear increase for x>20 mol% which suggested to be due to the replacement of B_2O_3 (0.002 Å^3 and 0.425) with higher electronic polarizability and basicity TeO_2 (0.242 Å^3 and 0.93) [17, 36]. Thus, the addition of higher polarizability cation reduced the influence of boron on electron cloud charge of oxygen ions which results in increased electronic polarizability and optical basicity of the glass. However, a slight slope changes in $\alpha_{O^{2-}}$ and Λ was observed at x=40 mol% (Figure 7) which suggested to be due to the large formation of NBO via TeO_3 and BO_3 units which possess high polarizability. NBO exhibit high iconicity indicating stronger electron donating power of oxide ion which results in enhancement of Λ.

Table 2. Variations of electronic polarizability ($\alpha_{O^{2-}}$), optical basicity (Λ), dielectric constant (ε) of $(80\text{-}x)B_2O_3\text{-}xTeO_2\text{-}10Li_2O\text{-}10Al_2O_3$ (x = 10−60 mol%) glass samples.

x (mol %)	$\alpha_{O^{2-}}$	Λ	ε
10	2.94	1.10	5.41
20	2.81	1.08	4.85
30	2.96	1.11	5.03
40	3.11	1.13	5.46
50	3.17	1.14	5.10
60	3.29	1.16	5.32

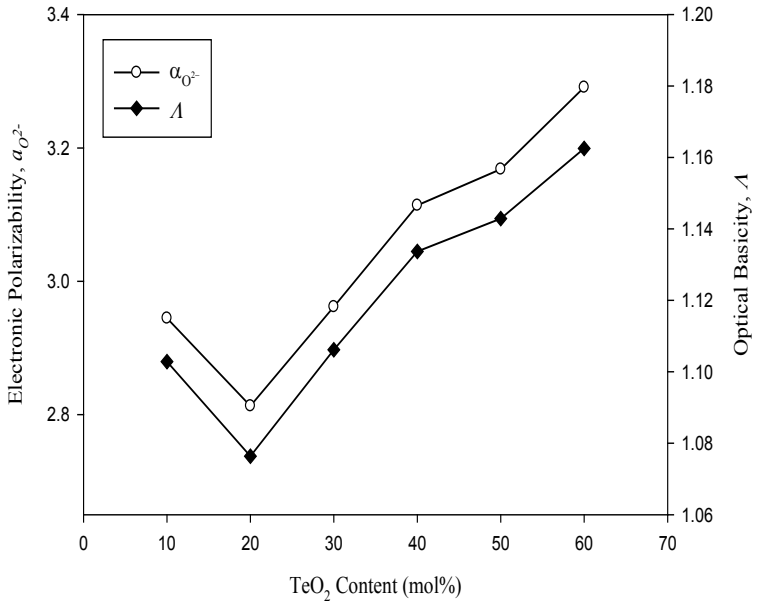

Fig. 7. Plot of $\alpha_{O^{2-}}$ and Λ with TeO_2 content of (80-x)B_2O_3-xTeO_2-10Li_2O-10Al_2O_3 (x=10−60 mol%) glass samples.

3.2. Radiation shielding parameters

It is necessary to have radiation shielding in order to protect people as well as technology from the highly unsafe ionizing radiation's effects. It is helpful to have information on the kind of shielding material, its thickness, the energy of radiation that needs to be shielded against, and the type of radiation. In order to get the required information about the suitable shielding materials, we must determine some attenuation factors of different materials. These factors are necessary for evaluating the overall efficacy of the shield in terms of minimizing the level of radiation that is exposed to the humans. The shielding factors are utilized in the planning and optimization of the shielding in attempt to achieve the highest expected degree of protection with the fewest possible resources and expenses. The amount by which the intensity of radiation is reduced when it travels through a shield material is measured using the attenuation factors. In this study, the Phy-X/PSD software was employed to determine the shielding parameters precisely [47].

One of the most common attenuation factors is the linear attenuation coefficient (LAC), which is the percentage of the photon that is absorbed by the shields for every unit of thickness that it possesses. The LAC depends on the radiation's energy, the shielding material's atomic number, and its density. Figure 8 plots the linear attenuation coefficient (LAC) of the glasses as a function of the incoming photon energy. As the energy of the radiation increases, all the LAC values decrease. The *x*=30 mol% sample starts out at 0.396 cm^{-1} and drops to 0.252 cm^{-1} at 0.511 MeV, 0.192 cm^{-1} at 0.826 MeV, 0.152 cm^{-1} at 1.275 MeV, while the *x*=50 mol% sample has the LAC values equal to 0.500, 0.296, 0.221, and 0.174 cm^{-1} at the same respective energies. This drop in LAC values with energy is similar to the trend found for MAC, which reaffirms the conclusion that the glasses can stop more photons at lower energies. Unlike the previous figure, however, there is a much greater difference between the LAC values at all energies, including at higher energies. For instance, at 0.347 MeV, the *x*=10 mol% sample has an LAC of 0.251 cm^{-1}, while the *x*=60 mol% sample has an LAC of 0.447 cm^{-1}, while at 1.333 MeV, they have LAC values equal to 0.126 cm^{-1} and 0.183 cm^{-1}, respectively. In short, increasing the TeO_2 content of the glass system leads to an improvement in the shielding ability of the glasses.

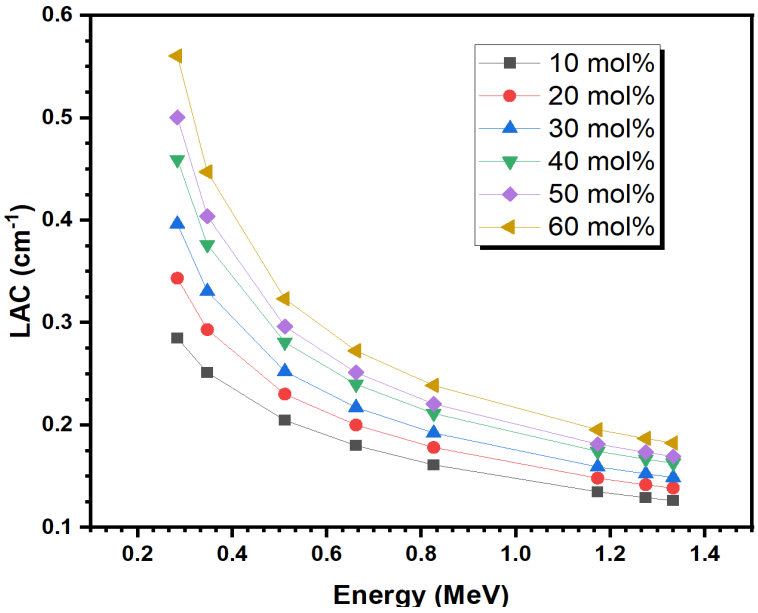

Fig. 8. The linear attenuation coefficient (LAC) against energy of (80-x)B_2O_3-xTeO_2-10Li_2O-10Al_2O_3 (x=10−60 mol%) glass samples.

By dividing the LAC for a given material by the density of the shielding material, the mass attenuation coefficient (MAC) for that material can be obtained through this formula given [48]:

$$MAC = \frac{LAC}{density} \tag{9}$$

The mass attenuation coefficients (MAC) of the glass samples are compared against incoming photon energy (Figure 9**)**. The greatest MAC values occur at the lowest tested energy, 0.2835 MeV, and decrease to their minimum at 1.333 MeV. Specifically, the 20 mol% glass sample has MAC values equal to 0.129, 0.087, 0.067, and 0.052 cm^2/g at 0.284, 0.511, 0.826, and 1.333 MeV, respectively. The inverse relationship between MAC and energy signifies that the shielding ability of the glasses is greatest against lower energy photons, and decreases with higher energy photons. Moreover, at all energies, the glass sample with 10 mol% TeO_2 has the lowest MAC, while the sample with 60 mol% TeO_2 has the highest MAC at all energies. This is most evident at 0.284 MeV, where the difference between the values is the highest. At this energy, the MAC values are equal to 0.119, 0.129, 0.137, 0.144, 0.150, and 0.155 cm^2/g for x=10-60 mol% TeO_2, respectively. At higher energies, such as at 1.333 MeV, the difference between the MACs is much smaller, varying at 0.053 cm^2/g for x=10 mol% to 0.050 for x=60 mol% of TeO_2, respectively. Therefore, at all energies, the 60 mol% TeO_2 glass has the best shielding ability, but its advantage is best observed against lower energy photons.

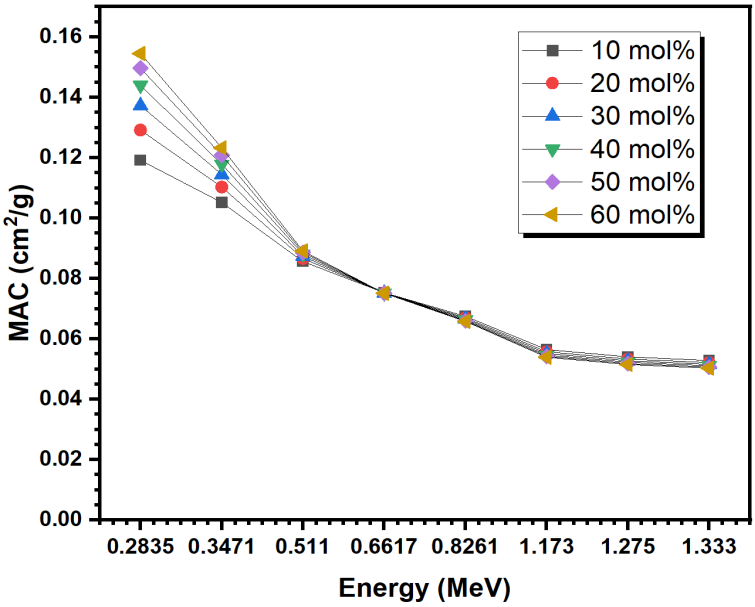

Fig. 9. The mass attenuation coefficients (MAC) against energy of (80-x)B_2O_3-xTeO_2-10Li_2O-10Al_2O_3 (x=10−60 mol%) glass samples.

Besides that, other attenuating factors also can be evaluated such as the half value layer (HVL). Radiation safety is reliant on a proper understanding of this concept. It is the thickness of a medium that halves the level of radiation that is transmitted through the medium while it is in place [49]. In addition to this, it could be utilized to estimate the amount of shielding that is necessary to reduce the quantity of radiation exposure to a healthy level and identify the degree to which specific photons can penetrate. Practically, we can compute the HVL for certain material using [50, 51]:

$$HVL = \frac{0.693}{LAC} \tag{10}$$

Figure 10 shows the half value layer (HVL) of the glasses as a function of increasing energy. At any single energy, the HVL of the glasses are in the order of 10 mol% > 20 mol% > 30 mol% > 40 mol% > 50 mol% > 60 mol%. For instance, at 0.511 MeV, they are equal to 3.387 cm, 3.009 cm, 2.745 cm, 2.467 cm, 2.338 cm, and 2.144 cm for *x*=10-60 mol%, respectively. Meanwhile, at 1.275 MeV, the HVL values are equal to 5.361 cm, 4.884 cm, 4.547 cm, 4.155 cm, 3.995 cm, and 3.707 cm for the same respective glasses. Therefore, by increasing the TeO_2 content of the glasses, the space-efficiency of the glasses improves. Furthermore, the HVL values are lowest at the lowest tested energies, and highest against higher energy photons. The *x*=20 mol% glass has an HVL of 2.018 cm at 0.284 MeV, and 4.998 cm at 1.333 MeV, while the *x*=50 mol% glass has an HVL of 1.385 and 4.090 cm at the same respective energies. Because HVL increases as the energy of the incoming photons increases, a thicker glass sample is required to attenuate the same number of higher energy photons.

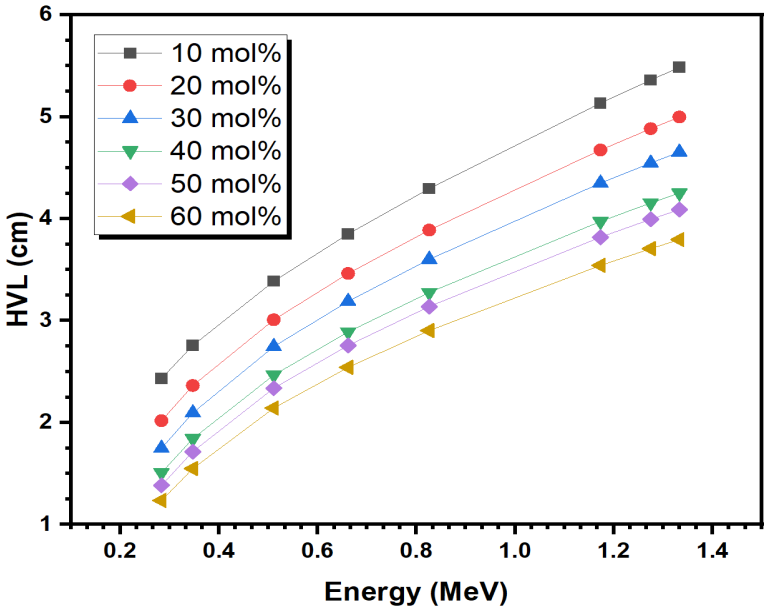

Fig. 10. The half value layer (HVL) against energy of (80-x)B_2O_3-xTeO_2-10Li_2O-10Al_2O_3 (x=10−60 mol%) glass samples.

The tenth value layer, or TVL, of the glasses evaluates how thick the glass samples need to be to reduce the level of radiation to one-tenth of its original value at a specific energy [52]. It can be calculated by using this relation [50]:

$$TVL = \frac{ln10}{\mu} \tag{11}$$

The TVL of the glasses against the energy of the photons are graphed in Figure 11. For every glass, its TVL values are higher than its HVL values, especially at higher energies. For instance, at 1.333 MeV, the TVL values are equal to 18.223 cm for *x*=10 mol%, 16.604 cm for *x*=20 mol%, 15.460 cm for *x*=30 mol%, 14.128 cm for *x*=40 mol%, 13.585 cm for *x*=50 mol%, and 12.608 cm for *x*=60 mol%. These results also reveal that the 60 mol% glass has the lowest TVL out of the investigated glasses, while the 10 mol% glass has the highest TVL. At lower energies, this trend also occurs, with TVL and TeO_2 content having an inverse relationship, although they are at their lowest. Specifically, at 0.284 MeV, the TVL values range between 4.108−8.083 cm and range between 12.608−18.223 cm at 1.333 MeV. Thus, increasing the TeO_2 content and decreases the energy of the incoming photons causes a thinner shield to be required to attenuate nine-tenths of the incoming radiation.

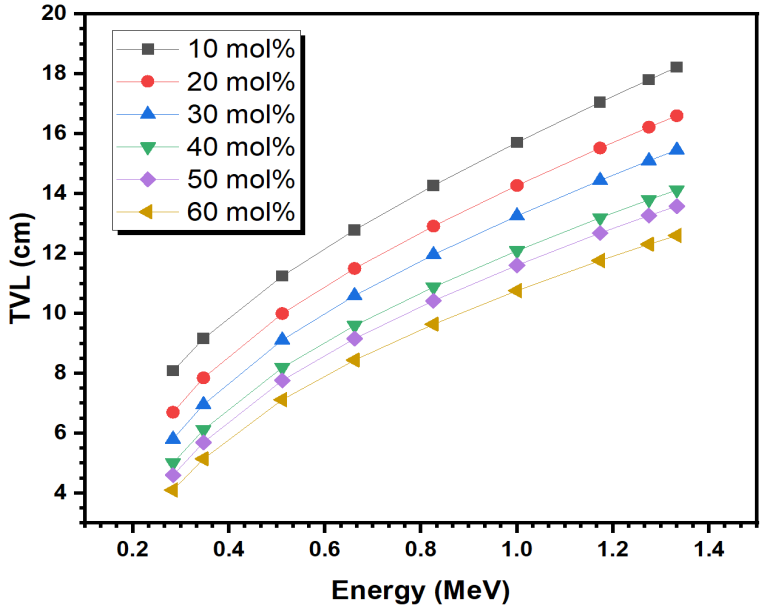

Fig. 11. The tenth value layer (TVL) against energy of (80-x)B_2O_3-xTeO_2-10Li_2O-10Al_2O_3 (x=10−60 mol%) glass samples.

The concept of the mean free path, also referred to as MFP, is essential for the investigation of transport mechanisms, especially in the areas of radiation protection. It is the distance a photon is capable of passing through a type of media before coming into contact with another photon [53]. The MFP is capable of providing information into the behavior of photons in a given medium and can be used to assess the performance of a specific material in terms of its ability to shield radiation. It is related to the LAC as in next equation [50]:

$$MFP = \frac{1}{LAC} \tag{12}$$

Figure 12 illustrates the mean free path, or MFP, of the investigated glasses against energy. The MFP of all six glasses is directly proportional to the energy of the incoming radiation. In other words, at lower energies such as 0.347 MeV, the MFP values are between 2.236 and 3.978 cm, while at higher energies such as 1.173 MeV they are between 5.112 cm and 7.407 cm. Higher energy photons tend to penetrate through the glasses more easily, which leads to less collisions, and thus a smaller distance between subsequent collisions, or MFP. Meanwhile, lower energy photons tend to collide more with the atoms in the glasses, leading to greater attenuation, and a better shielding ability. The lower MFP without changing the energy of the incoming photons, the TeO_2 content can be increased while substituting the B_2O_3 of the glasses. At 0.662 MeV, the glass with 10 mol% of TeO_2 has MFP value of 5.555 cm, which drops to 4.996 cm for *x*=20 mol%, 4.603 cm for *x*=30 mol%, 4.169 cm for *x*=40 mol%, 3.979 cm for *x*=50 mol%, and 3.668 cm for *x*=60 mol%. The increased TeO_2 raises the density of the glasses, increasing the probability of collisions within the material, and thus decreasing MFP. Therefore, to optimize the shielding ability of the glass system, the TeO_2 content should be maximized, such as for *x*=60 mol%.

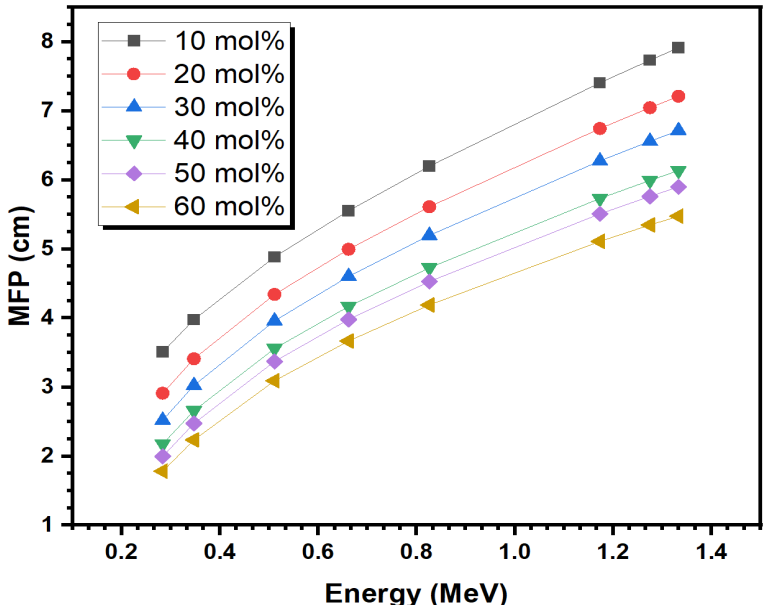

Fig. 12. The mean free path (MFP) against energy of (80-x)B_2O_3-xTeO_2-10Li_2O-10Al_2O_3 (x=10−60 mol%) glass samples.

Last but not least, the effective atomic number, Zeff is a radiation parameter that correlates with the elements of a material and affected by the incoming energy. Higher Zeff material is encouraged as it helps the shielding properties with higher number of electrons per atom [54]. It can be acquired by using the following relation [48]:

$$\sigma_t = \frac{M(\mu/\rho)}{N_A}, \tag{13}$$

$$\sigma_a = \frac{\sigma_t}{\sum_i n_i}, \tag{14}$$

$$\sigma_e = \frac{1}{N_A}\sum_i \frac{f_i A_i}{Z_i}(\mu_m)_i \tag{15}$$

$$Z_{eff} = \frac{\sigma_a}{\sigma_e} \tag{16}$$

where f_i is the fractional abundance of the element *i* relative to the number of atoms providing that $\sum f_i = 1$, A_i is the atomic weight, and Z_i is the atomic number.

Figure 13 demonstrates the Z_{eff} of the glasses as a function of energy. The Z_{eff} values can be split into two general regions. At low energies, the Z_{eff} of the glasses are at their maximum, and decrease at a relatively rapid rate. For instance, glass with *x*=40 mol% has the Z_{eff} value drops from 15.64 to 14.32 at 0.284 MeV and 0.347 MeV, respectively, and then to 12.97 at 0.511. As energy further increases, this decrease in Z_{eff} rapidly slows down, and Z_{eff} remains almost constant with energy. Continuing, 40 mol%'s Z_{eff} is equal to 12.53, 12.30, and 12.07 at 0.662, 0.826, and 1.333 MeV, respectively. The trends associated with these regions are caused by the photoelectric effect and the Compton scattering effect, respectively, which have different relationships with energy. The figure also shows that the 60 mol% glass has the highest Z_{eff} at all energies. This result can be attributed to the fact that Te has a higher atomic number than B (52 vs. 6), so substituting more TeO_2 for B_2O_3 raises the atomic number of the glass system. Because a higher Z_{eff} is typically associated with a more efficient material, increasing the TeO_2 content of the glasses leads to an improvement in the attenuation capability of the glass system.

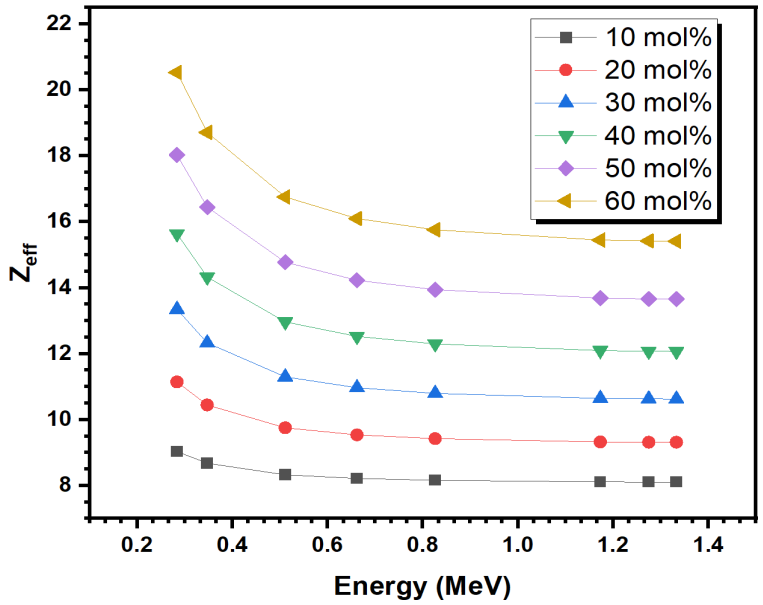

Fig. 13. The effective atomic number (Z_{eff}) against energy of (80-x)B_2O_3-xTeO_2-10Li_2O-10Al_2O_3 (x=10−60 mol%) glass samples.

4. Conclusions

The optical properties of (80−*x*)B_2O_3-*x*TeO_2-10Li_2O-10Al_2O_3 (*x*=10−60 mol%) MGF glasses were determined. Optical band gap, E_{opt} showed minimum values at *x*=40 mol% due to high formation of NBO as indicated by BO_3 and TeO_3 concentrations, requiring less energy to induce electron excitation. The *n* value has shown contrasting behavior than E_{opt} where a maximum was seen at *x*=40 mol% due to the increase in NBO which possess high polarizability. The increase in NBO also leads to a maximum in E_u at the same location which indicates large concentration of defects. A slight slope changes also observed at *x*=40 mol% for $\alpha_{O^{2-}}$ and Λ due to the large concentration of NBO which possess high polarizability and strong electron donor power. Phy-X/PSD simulation software has been employed to investigate the radiation shielding properties of (80−*x*)B_2O_3-*x*TeO_2-10Li_2O-10Al_2O_3 (*x*=10−60 mol%) MGF glasses at 0.284 MeV to 1.333 MeV.

Increasing TeO_2 content in the glass has improved the MAC and LAC values where highest value was recorded at *x*=60 mol% and glass samples performed best at lower energy region. Meanwhile, higher density of TeO_2 has contributed to the enhancement in HVL, TVL and MFP values as TeO_2 added where lowest value were seen for these parameters at *x*=60 mol%; hence, effectively shielding radiation at thinner dimension. Lastly, continuous substitution of B_2O_3 with TeO_2 has improved the Z_{eff} values due to higher atomic number of Te over B with better value obtained at *x*=60 mol%; thus, indicates better attenuation capabilities of the glass system.

Acknowledgements

The authors express gratitude to the Research Management Centre (RMC) and Universiti Teknologi MARA, Malaysia for assistance throughout the research. This study was financially supported by Strategic Research Partnership (SRP) Grant under Universiti Teknologi MARA and Universiti Teknologi Malaysia with file numbers of 100-RMC 5/3/SRP GOV (005/2021) and Q.J130000.3054.03M63, respectively.

References

[1] M. Pal, B. Roy, and M. Pal, Journal of Modern Physics, (2011), (2011).

[2] K. J. Rao, "Structural chemistry of glasses," Elsevier, (2002).

[3] A. K. Varshneya, "Fundamentals of inorganic glasses," Elsevier, (2013).

[4] K. Maheshvaran and K. Marimuthu, Journal of luminescence, (132), 2259(2012); https://doi.org/10.1016/j.jlumin.2012.04.022

[5] K. Selvaraju and K. Marimuthu, Journal of luminescence, (132), 1171 (2012); https://doi.org/10.1016/j.jlumin.2011.12.056

[6] K. Selvaraju, K. Marimuthu, T. Seshagiri, and S. Godbole, Materials Chemistry and Physics, (131), 204(2011); https://doi.org/10.1016/j.matchemphys.2011.09.006

[7] N. S. Sabri, A. Yahya, and M. K. Talari, Transactions of the Indian Institute of Metals, (70), 557(2017); https://doi.org/10.1007/s12666-017-1043-8

[8] M. Storek, M. Adjei-Acheamfour, R. Christensen, S. W. Martin, and R. Böhmer, The Journal of Physical Chemistry B, (120), 4482(2016); https://doi.org/10.1021/acs.jpcb.6b00482

[9] Y. Saddeek, K. Aly, K. Shaaban, A. M. Ali, M. M. Alqhtani, A. M. Alshehri, et al., Journal of Non-crystalline Solids, (498), 82(2018); https://doi.org/10.1016/j.jnoncrysol.2018.06.002

[10] K. A. Naseer, K. Marimuthu, M. S. Al-Buriahi, A. Alalawi, and H. O. Tekin, Ceramics International, (47), 329(2021); https://doi.org/10.1016/j.ceramint.2020.08.138

[11] G. Ferlat, A. P. Seitsonen, M. Lazzeri, and F. Mauri, Nature materials, (11), 925(2012); https://doi.org/10.1038/nmat3416

[12] S. Rani, S. Sanghi, N. Ahlawat, and A. Agarwal, Journal of Alloys and Compounds, (597), 118(2014); https://doi.org/10.1016/j.jallcom.2014.01.211

[13] P. Pascuta, G. Borodi, and E. Culea, Journal of Non-Crystalline Solids, (354), 5475(2008); https://doi.org/10.1016/j.jnoncrysol.2008.09.010

[14] Y. Yang, Y. Liu, P. Cai, R. Maalej, and H. J. Seo, Journal of Rare Earths, (33), 939(2015); https://doi.org/10.1016/S1002-0721(14)60509-3

[15] Z. A. Said Mahraz, M. R. Sahar, S. K. Ghoshal, and M. Reza Dousti, Journal of Luminescence, (144), 139(2013); https://doi.org/10.1016/j.jlumin.2013.06.050

[16] K. Selvaraju and K. Marimuthu, Journal of Alloys and Compounds, (553), 273(2013); https://doi.org/10.1016/j.jallcom.2012.11.150

[17] R. Hisam and A. K. Yahya, Results in Physics, (13), 102219(2019); https://doi.org/10.1016/j.rinp.2019.102219

[18] N. Ahlawat, S. Sanghi, A. Agarwal, and R. Bala, Journal of Molecular Structure, (963), 82(2010); https://doi.org/10.1016/j.molstruc.2009.10.018

[19] D. Saritha, Y. Markandeya, M. Salagram, M. Vithal, A. Singh, and G. Bhikshamaiah, Journal of Non-Crystalline Solids, (354), 5573(2008); https://doi.org/10.1016/j.jnoncrysol.2008.09.017

[20] O. Ueda and S. J. Pearton, Materials and reliability handbook for semiconductor optical and electron devices, (2013); https://doi.org/10.1007/978-1-4614-4337-7

[21] S. Y. Marzouk, R. Seoudi, D. A. Said, and M. S. Mabrouk, Optical Materials, (35), 2077(2013); https://doi.org/10.1016/j.optmat.2013.05.023

[22] S. B. Mallur, T. Czarnecki, A. Adhikari, and P. K. Babu, Materials Research Bulletin, (68), 27(2015); https://doi.org/10.1016/j.materresbull.2015.03.033

[23] M. Abdel-Baki and F. El-Diasty, Current Opinion in Solid State and Materials Science, (10), 217(2006); https://doi.org/10.1016/j.cossms.2007.08.001

[24] M. Azlan, M. Halimah, S. Shafinas, W. Daud, and H. Sidek, Solid State Science and Technology, (22), 148(2014).

[25] K. M. Kaky, M. Sayyed, F. Laariedh, A. H. Abdalsalam, H. Tekin, and S. Baki, Applied Physics A, (125), 1(2019); https://doi.org/10.1007/s00339-018-2329-3

[26] N. F. Mott and E. A. Davis, "Electronic processes in non-crystalline materials," Oxford University Press, (2012).

[27] R. López and R. Gómez, Journal of Sol-Gel Science and Technology, (61), 1(2012); https://doi.org/10.1007/s10971-011-2582-9

[28] M. Ismail, S. N. Supardan, A. K. Yahya, and R. Abd-Shukor, International Journal of Materials Research, (106), 893(2015); https://doi.org/10.3139/146.111250

[29] S. Sanghi, S. Duhan, A. Agarwal, and P. Aghamkar, Journal of Alloys and Compounds, (488), 454(2009); https://doi.org/10.1016/j.jallcom.2009.09.009

[30] C. Zainudin, R. Hisam, M. Yusof, A. Yahya, and M. Halimah, Materials Research Express, (4), 105204(2017); https://doi.org/10.1088/2053-1591/aa9233

[31] H. M. Oo, H. Mohamed-Kamari, and W. M. D. Wan-Yusoff, International Journal of Molecular Sciences, (13), 4623(2012); https://doi.org/10.3390/ijms13044623

[32] S. Hajer, M. Halimah, Z. Azmi, and M. Azlan, Chalcogenide Letters, (11), (2014).

[33] V. Dimitrov and S. Sakka, Journal of Applied Physics, (79), 1736(1996); https://doi.org/10.1063/1.360962

[34] R. El-Mallawany, Tellurite glass smart materials: applications in optics and beyond, Springer, (2018); https://doi.org/10.1007/978-3-319-76568-6

[35] P. G. Pavani, K. Sadhana, and V. C. Mouli, Physica B: Condensed Matter, (406), 1242(2011); https://doi.org/10.1016/j.physb.2011.01.006

[36] V. Dimitrov and T. Komatsu, An interpretation of optical properties of oxides and oxide glasses in terms of the electronic ion polarizability and average single bond strength (review), (2010).

[37] M. A. Hazlin, M. Halimah, F. Muhammad, and M. Faznny, Physica B: Condensed Matter, (510), 38(2017); https://doi.org/10.1016/j.physb.2017.01.012

[38] S. N. Mohamed and A. K. Yahya, Ionics, (24), 2647(2017).

[39] F. Urbach, Physical Review, (92), 1324(1953); https://doi.org/10.1103/PhysRev.92.1324

[40] T. R. Rao, C. V. Reddy, C. R. Krishna, D. Sathish, P. S. Rao, and R. Ravikumar, Materials Research Bulletin, (46), 2222(2011); https://doi.org/10.1016/j.materresbull.2011.09.007

[41] S. Meena and B. Bhatia, J. Pure Appl. Ind. Phys., (6), 175(2016).

[42] N. M. Samsudin, R. Hisam, and A. K. Yahya, Ionics, (27), 619(2021).

[43] D. Thombre and M. Thombre, International Journal of Engineering Research and Development, (10), 9(2014).

[44] R. Hisam, A. K. Yahya, H. M. Kamari, Z. A. Talib, and R. H. Y. Subban, Materials Express, (6), 149(2016); https://doi.org/10.1166/mex.2016.1286

[45] J. Duffy and M. D. Ingram, Journal of Non-Crystalline Solids, (21), 373(1976); https://doi.org/10.1016/0022-3093(76)90027-2

[46] J. A. Duffy and M. D. Ingram, The Journal of Chemical Physics, (54), 443(1971); https://doi.org/10.1063/1.1674635

[47] E. Şakar, Ö. F. Özpolat, B. Alım, M. I. Sayyed, and M. Kurudirek, Radiation Physics and Chemistry, (166), 108496 (2020); https://doi.org/10.1016/j.radphyschem.2019.108496

[48] G. Lakshminarayana, S. O. Baki, A. Lira, M. I. Sayyed, I. V. Kityk, M. K. Halimah, et al., Journal of Materials Science, (52), 7394(2017); https://doi.org/10.1007/s10853-017-0974-0

[49] M. M. Naaim, M. F. Malek, M. I. Sayyed, N. F. M. Sahapini, and R. Hisam, Ceramics International, (2022).

[50] P. Kaur, K. J. Singh, M. Kurudirek, and S. Thakur, Spectrochim Acta A Mol Biomol Spectrosc, (223), 117309(2019); https://doi.org/10.1016/j.saa.2019.117309

[51] S. J. Japari, M. I. Sayyed, A. K. Yahya, A. L. Anis, S. M. Iskandar, M. H. M. Zaid, et al., Results in Physics, (22), 103946(2021); https://doi.org/10.1016/j.rinp.2021.103946

[52] S. Kaewjaeng, N. Chanthima, J. Thongdang, S. Reungsri, S. Kothan, and J. Kaewkhao, Materials Today: Proceedings, (43), 2544(2021); https://doi.org/10.1016/j.matpr.2020.04.615

[53] S. Shuhaimi, M. Sayyed, F. Hila, A. Anis, S. Iskandar, M. Zaid, et al., Physica Scripta, (97), 045804(2022).

[54] K. M. Kaky, M. I. Sayyed, F. Laariedh, A. H. Abdalsalam, H. O. Tekin, and S. O. Baki, Applied Physics A, (125), (2018); https://doi.org/10.1007/s00339-018-2329-3